Analytical prediction and experimental validation for longitudinal control of cable oscillations

Vincenzo Gattulli, Rocco Alaggio, Francesco Potenza

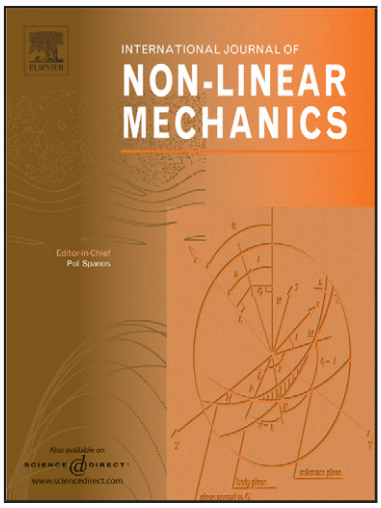

www.elsevier.com/locate/nlm

Analytical prediction and experimental validation for longitudinal control of cable oscillations

Vincenzo Gattulli, Rocco Alaggio, Francesco Potenza

PII: S0020-7462(07)00196-5
DOI: doi:10.1016/j.ijnonlinmec.2007.10.001
Reference: NLM 1405

To appear in: *International Journal of Non-Linear Mechanics*

Received date: 19 December 2006
Revised date: 17 September 2007
Accepted date: 1 October 2007

Cite this article as: Vincenzo Gattulli, Rocco Alaggio and Francesco Potenza, Analytical prediction and experimental validation for longitudinal control of cable oscillations, *International Journal of Non-Linear Mechanics* (2007), doi:10.1016/j.ijnonlinmec.2007.10.001

Analytical Prediction and Experimental Validation for Longitudinal Control of Cable Oscillations

Vincenzo Gattulli * Rocco Alaggio † Francesco Potenza ‡

Submitted: *December 19, 2006*

Number of pages: 36

Number of tables: 1

Number of figures: 12

*Dipartimento di Ingegneria delle Strutture, delle Acque e del Terreno, Università di L'Aquila, 67040 Monteluco di Roio (L'Aquila), Italy (gattulli@ing.univaq.it, tel. -39-0862-434511, fax -39-862-434548, Corresponding Author)

†Dipartimento di Ingegneria delle Strutture, delle Acque e del Terreno, Università di L'Aquila, 67040 Monteluco di Roio (L'Aquila), Italy

‡Dipartimento di Ingegneria delle Strutture, delle Acque e del Terreno, Università di L'Aquila, 67040 Monteluco di Roio (L'Aquila), Italy

Abstract

The paper summarizes the knowledge acquired from the analytical studies and the experimental implementation of a longitudinal noncollocated control strategy for the reduction of cable oscillations. The control is introduced by imposing a longitudinal action at one support based on the knowledge of transverse displacements and velocities of a few selected points. A spatially one-dimensional continuous model of a suspended cable has been used to describe the main features of the noncollocated longitudinal active control strategy. A discrete modal representation has permitted the introduction of suitable nonlinear state-feedback controllers. The results have been used to derive an implementable strategy, based on direct output feedback, which preserves the main previous control features. A physical model of an actively controlled cable has been used to demonstrate the control effectiveness of the proposed strategy through a large campaign of experiments, conducted in various frequency ranges and amplitude levels including meaningful external resonance conditions. The responses predicted by the analytical model and the experimental results show good qualitative agreement with one another, in both the uncontrolled and controlled experienced cable dynamics.

Key words: Active Control, Nonlinear Dynamics, Cables, Experimental Dynamics

1 Introduction

The active control of cable oscillations presents a challenging research problem due to its twofold technical and theoretical nature involving control and nonlinear dynamics. The problem is a worthwhile challenge because practically implementable control techniques to suppress cable vibrations will enhance cable structural efficiency, preventing degradation and fatigue damage, and will increase serviceability performance. Yet, the variety of nonlinear phenomena that cables present, along with the complexity of their mathematical models [1], introduces appreciable novelty to the control problem.

Research on cable dynamics is primarily motivated by recurrent vibration phenomena experienced in different engineering applications involving these important structural elements. Different methods have been proposed to reduce such vibrations. Passive dampers acting in the transverse direction are devices most commonly utilized and they have recently been enhanced through the use of semi-active technology [2]. However, the location of these dampers, generally close to the cable support, limits the maximum achievable modal damping, especially in long cables [3]. A recent alternative approach is the use of an active control scheme utilizing either a transverse [4, 5] or a longitudinal [6, 7] boundary motion. In the first case, a collocated control configuration is proposed with an imposed out-of-plane movement of the support based on position, velocity and angle measure [4]. The stability properties of the controlled system furnish the basis for an adaptive strategy to control out-of-plane cable oscillations [5]. In the second case, a longitudinal action at the support is used to reduce transverse vibrations, taking advantage of the fact that longitudinal motion is coupled with transverse motion in the range of small amplitude vibrations, as well. Both noncollocated and collocated control configurations have been considered. In the case of the noncollocated control configuration, the longitudinal action relies on the measured transverse displacements and velocities of some monitored points; in the collocated configuration, it relies only on physical quantities in the longitudinal direction at the support. Different effects evidenced due to the longitudinal action [6, 7] are known as active stiffness control, when associated with cable stretching, and active sag induced force control, when associated with the initial curvature of the cable. The aim of the collocated configuration is to prevent spillover instability, but it has primarily been used to reduce in-plane oscillations [8]. Noncollocated control strategies have also been considered in slack [9] and shallow [10] cables. A previous study by one of the authors has shown that the longitudinal active control scheme requires a careful analysis because geometric nonlinearities coupled with control feedback may introduce non-dissipative terms, producing some undesirable effects [9]. Thus, the state-feedback in a polynomial form was analyzed looking separately at the effects of the different terms. In

particular, it has been shown that linear and quadratic velocity terms can be effective in reducing in-plane oscillations, while quadratic terms have to be used for the out-of-plane components. Another possibility is a feedback linearization of the system, which offers advantages and disadvantages, as shown in [11]. In the cited work, local and global analysis of the controllability of the nonlinear discrete system of the cable have been developed. Hence, a state-feedback cancelation of the nonlinear terms describing the cable elongation is presented, showing the possibility of obtaining a simpler controlled dynamical system represented in a bilinear form, which assures global asymptotic stabilization of free oscillations in the cable. Finally, in order to evaluate control spillover effects inherent to the proposed noncollocated scheme an enlarged 8-*dofs* model is considered. This model numerically evidences the absence of instabilities in the experienced control region.

The present paper demonstrates of the ability of multimodal longitudinal active control to reduce nonlinear cable oscillations. Results previously obtained both theoretically and numerically [7, 9, 11] are here extended by deeply considering the contribution of the anti-symmetric modes to the cable dynamics, which contribution is strongly evidenced in the novel experimental validation of the studied control strategies. In this respect, an implementable noncollocated control law based on direct-output feedback is presented showing that this approach preserves all the previous features of the developed control algorithms. Then, different refined reduced discrete models, with an increasing number of modes accounted in the description of the relevant cable dynamics, has been used to evaluate numerically the performance of the selected control laws. These analyses have been driven by the dynamics experienced in the laboratory tests. Indeed, despite the nominal absence of internal resonance for the selected cable, the experienced dynamics have shown, under in-plane harmonically-forced oscillations, a rich and evident modal coupling between the first two in-plane and two out-of-plane modes, respectively. The main modal interaction phenomena have been described constructing the frequency response curves, namely *frcs* to in-plane symmetric harmonic load, for discrete cable models containing an increasing number of modal components. The numerical findings have been confirmed by experimental results showing that in a wide experienced frequency range of the symmetric harmonic force, selected around the first symmetric modes, a rich modal interaction involving mainly the first four modes can be found even in the absence of internal resonance conditions. These modal components are opportunely captured in the experiments by means of two biaxial follower cameras positioned in two points at $\ell/4$ and $3/4\ell$. The control strategy has been based on a single longitudinal action driven by the direct-output nonlinear feedback. On the basis of the measured four transverse components, the strategy has shown control capability in the entire experienced

frequency range, overcoming all the encountered motions from the classical symmetric in-plane type to more complicated spatial motion with both symmetric and anti-symmetric components.

2 Analytical model and control strategy

The static equilibrium configuration of a cable suspended between two fixed horizontal supports can be described by a curve that lies in the vertical plane (Oxy in Fig. 1). By referring to taut and shallow cables (i.e. $d/\ell \leq 1/8$, where d is the cable sag and ℓ is the distance between the two supports), the configuration under self-weight can be described by a parabolic function, $y(x) = 4d\left[x/\ell - (x/\ell)^2\right]$, with constant horizontal tension H, assumed to describe the initial tension N_0, ($N_0(s) \simeq H$).

The evaluation of the static reference configuration C^0 described by the parabolic function $y(x)$, permits the derivation of the dynamic varied configuration C^1 through the displacement components $u(x,t)$, $v(x,t)$ and $w(x,t)$ along the co-ordinate axes x,y and z, respectively.

Following [12], the Lagrangian measure of strain is assumed:

$$e(x,t) = u' + y'v' + \frac{1}{2}\left(v'^2 + w'^2\right) \tag{1}$$

the equations of motion of the system are obtained through the extended Hamilton's principle,

$$\begin{aligned} &m\ddot{u} + \mu_u\dot{u} - [EAe]' = 0 \\ &m\ddot{v} + \mu_v\dot{v} - [Hv' + EA\,(y' + v')\,e]' = 0 \\ &m\ddot{w} + \mu_w\dot{w} - [Hw' + EAw'e]' = 0 \end{aligned} \tag{2}$$

where E is the modulus of elasticity, A is the area of the cross section, m, μ_u, μ_v and μ_w are the mass and damping coefficients of the cable for unit length; a dot and a prime indicate derivatives with respect to time t and the abscissa x, respectively. The assumption has been introduced that the gradient of the horizontal component of the dynamic displacement is smaller than the gradient of the transversal components ($u' \ll v', w'$), and $y' \ll 1$, $H/EA \ll 1$, and the problem is completed by boundary conditions in $0, \ell$ which take into account both the control action u_c and the vertical synchronous support motion v_g producing the in-plane excitation. In particular, a longitudinal displacement $u_c(t)$ of one support ($x = \ell$) is imposed as a control action, assuming that $u_c/\ell \ll 1$ for all t. With this type of control and external excitation the differential equation of motion (2) is not changed, while the following boundary conditions

hold:

$$
\begin{aligned}
&u(0,t)=0, \quad u(l,t)=u_c(t)\\
&v(0,t)=v_g(t), \quad v(l,t)=v_g(t)\\
&w(0,t)=0, \quad w(l,t)=0
\end{aligned}
\tag{3}
$$

Under the previous assumptions regarding the cable geometry and taking a slow dependence on time of $u_c(t)$ with respect to the longitudinal frequencies, $u(x,t)$ can be eliminated by a standard condensation procedure leading to a definition of a constant elongation $\bar{e}$ as

$$
\bar{e}(t)=\left[u_c/\ell+1/\ell\int_0^\ell\left(y'v'+\frac{v'^2+w'^2}{2}\right)dx\right] \tag{4}
$$

Hence, the two integral-differential equations of motion in the transverse displacements are obtained:

$$
\begin{aligned}
&m\ddot{v}+\tilde{\mu}_v\dot{v}-\left[Hv'+EA\left(y'+v'\right)\bar{e}\right]'=0\\
&m\ddot{w}+\tilde{\mu}_w\dot{w}-\left[Hw'+EAw'\bar{e}\right]'=0
\end{aligned}
\tag{5}
$$

Besides the well known quadratic and cubic interaction terms of an uncontrolled cable, Eqs.(5) show that the imposed longitudinal control motion, u_c, enters as a parametric action in the out-of-plane motion and contemporary with parametric and external actions in the in-plane motion. On the basis of the longitudinal dynamic strain measure, the reaction at the support can ideally be decomposed into three different terms: $N(t)=H+EA\bar{e}(t)=H+N_c+N_d$ namely the static reaction H, the control force N_c and the dynamic reaction N_d.

2.1 Discretized model

A non-dimensional form of the equations is obtained by normalizing the variables with respect to the cable length and the first in-plane frequency ω_{1v} of the cable, as reported in Appendix; however, in the following, when there is no risk of confusion, the tilde will be omitted and a dot will indicate derivative with respect to τ. In order to describe the non-linear oscillations of the system forced by the imposed in-plane support motion and controlled by longitudinal action, the different contributions to the in-plane displacements in the Hamiltonian functional have been distinguished

$$
v(x,t)=v_r(x,t)+v_g(t) \tag{6}
$$

where subscript r and g respectively denote the relative vertical displacement and the rigid uniform translation induced by vertical support motion. The vertical relative displacement component and the absolute horizontal component are described by the expansion

$$v_r(x,t) = \sum_{i=1}^{n_v} \varphi_i(x) q_{iv}(\tau) \quad , \quad w(x,t) = \sum_{i=1}^{n_w} \psi_i(x) q_{iw}(\tau) \tag{7}$$

where φ_i and ψ_i are the eigenfunctions of the linearized equations of motion (5) with the ω_{iv} and ω_{iw} frequencies in a ratio that depends on the non-dimensional Irvine parameter; the use of the Galerkin method leads to the following expanded expression for the constant elongation

$$\bar{e}(t) = \sum_{j=1}^{n_v} \mathrm{b_{1j}} q_{jv} + \sum_{i=1,j=1}^{n_v} \mathrm{b_{2ij}} q_{iv} q_{jv} + \sum_{i=1}^{n_w} \mathrm{b_{3i}} q_{iw}^2 + u_c = \phi(q_i, q_j) + u_c \tag{8}$$

Thus, the following nonlinear ordinary differential equations describe the motion:

$$\begin{aligned} &\ddot{q}_{iv} + \zeta_{ijv}\dot{q}_{iv} + \sum_{j=1}^{n_v} \mathrm{a_{0ij}} q_{jv} + (\mathrm{a_{1i}} + \sum_{j=1}^{n_v} \mathrm{a_{2j}} q_{jv})\bar{e} = p_i \ddot{v}_g \\ &\ddot{q}_{iw} + \zeta_{ijw}\dot{q}_{iw} + \omega_{iw}^2 q_{iw} + \mathrm{a_{3i}} q_{iw}\bar{e} = 0 \end{aligned} \tag{9}$$

where the in-plane cable frequency is obtained as $\omega_{iv}^2 = (a_{0ii} + a_{1i}b_{1i})$ while ω_{iw} is the out-of-plane frequency; the linear off-diagonal terms $(a_{0ij} + a_{1i}b_{1j}) = 0$ due to eigenfunction orthogonality. The expression of non-linear coefficients $a_{0ij},\ a_{1i},\ a_{2j},\ a_{3i},\ b_{1j},\ b_{2ij},\ b_{3i}$, together with the modal damping coefficients $\zeta_{ijv},\ \zeta_{ijw}$ and the modal participation factor p_i are reported in the Appendix.

In the following nonlinear analysis, the displacement function has been described by a four-mode expansion, involving the first two in-plane and out-of-plane modes. The analysis conducted on the effects of a full-state feedback will be useful to provide a more realistic output feedback control directly related to the output measured quantities.

2.2 Control strategy

- Linear and nonlinear velocity state feedback

A combination of both measured response components is considered in order to realize an effective feedback control in both in-plane and out-of-plane oscillations. On the basis of results obtained by different polynomial laws, [9], a control law has been selected which includes a linear and quadratic enhanced velocity feedback control in the in-plane component and quadratic enhanced control in the out-of-plane component (LQC):

$$u_{LQC}(t) = \sum_{i=1}^{n_v} \alpha_{vli}\dot{q}_{iv} + \sum_{i=1}^{n_v} \alpha_{vqi} q_{iv}\dot{q}_{iv} + \sum_{i=1}^{n_w} \alpha_{wqi} q_{iw}\dot{q}_{iw} \tag{10}$$

where α_{vli}, α_{vqi} and α_{wqi} are positive gain coefficients. However we will often refer in the following to the simple (LC), (LQC$_{in}$), (LQC$_{out}$) feedbacks, such as:

$$u_{LC}(t) = \alpha_{vl}\dot{q}_{1v}; \quad u_{LQCin}(t) = \alpha_{vl}\dot{q}_{1v} + \alpha_{vq}q_{2v}\dot{q}_{2v}; \quad u_{LQCout}(t) = \alpha_{vl}\dot{q}_{1v} + \alpha_{wq}q_{1w}\dot{q}_{1w} \tag{11}$$

- *State feedback bilinearization*

Looking at the structure of the equation of motion (9), a control strategy may be developed by observing that the system can be transformed into a bilinear form by a particular choice of the control feedback. Introducing the control law (BL)

$$u_{BL}(t) = -\phi(q_{iv}, q_{iw}) + \bar{u}_c \tag{12}$$

the feedback cancelation of the scalar function $\bar{e}$ representing the elongation may be obtained, leading to a bilinear dynamical system controlled only by the second added term, $\bar{u}_c$, in the equation (12):

$$\begin{aligned} &\ddot{q}_{iv} + \mu_{iv}\dot{q}_{iv} + \sum_{j=1}^{n_v} \mathrm{a_{0ij}} q_{jv} + (\mathrm{a_{1i}} + \sum_{j=1}^{n_v} \mathrm{a_{2j}} q_{jv})\bar{u}_c = p_{iv} \\ &\ddot{q}_{iw} + \mu_{iw}\dot{q}_{iw} + \omega_{iw}^2 q_{iw} + \mathrm{a_{3k}} q_{iw}\bar{u}_c = 0 \end{aligned} \tag{13}$$

The feedback bilinearization, resulting in equation (13), permits the design of the control term, $\bar{u}_c$, such that the static equilibrium configuration is globally stable; following the work [13] a suitable expression for $\bar{u}_c$ can be given, similar to equation (10).

- *Linear and nonlinear direct output-feedback*

The analytical results obtained through the use of state-feedback control laws, such as asymptotic stability and optimal selection of the control gains in the case of the high-dimensional state model, are not implementable in an experimental control system where amplitude is not measurable. However, the previous results can be used to propose an enhanced direct output feedback (EDO), for which performance similar to that obtained by the state-feedback controller is expected in the explored range of dynamics. In particular, we have selected a measurable output of the system that can give a good, direct approximation of the four fundamental modal amplitudes primarily involved in the cable dynamics. Considering two symmetric points with respect to the midspan, e.g. at $x = \ell_1 = \frac{1}{4}\ell$ and $x = \ell_2 = \frac{3}{4}\ell$, and measuring the four transversal components $\{v(\ell_1, t), w(\ell_1, t), v(\ell_2, t), w(\ell_2, t)\}$, the following system output can be

defined as a function of the system state described by the modal amplitudes q_{iv} and q_{iw}, as

$$\boldsymbol{\eta}(q_{iv}, q_{iw}) = \left\{ \begin{array}{c} \eta_{1v} \\ \eta_{2v} \\ \eta_{1w} \\ \eta_{2w} \end{array} \right\} = \frac{1}{2} \left\{ \begin{array}{c} v\left(\ell_1, t\right) + v\left(\ell_2, t\right) \\ v\left(\ell_1, t\right) - v\left(\ell_2, t\right) \\ w\left(\ell_1, t\right) + w\left(\ell_2, t\right) \\ w\left(\ell_1, t\right) - w\left(\ell_2, t\right) \end{array} \right\} \simeq \left\{ \begin{array}{c} q_{1v} \\ q_{2v} \\ q_{1w} \\ q_{2w} \end{array} \right\} + o(q_{3v}, ...; q_{3w}, ...) \tag{14}$$

The above defined output vector can easily be differentiated with respect to time through a digital implementable procedure furnishing the derivative in time vector $\dot{\boldsymbol{\eta}}$. On the basis of the availability of all components of the two vectors $\boldsymbol{\eta}$ and $\dot{\boldsymbol{\eta}}$, the following enhanced direct output control law (EDO) may be introduced,

$$u_{EDO}(t) = \alpha_{vl}\eta_{1v} + \alpha_{vq}\,\eta_{2v}\dot{\eta}_{2v} + \alpha_{wqs}\,\eta_{1w}\dot{\eta}_{1w} + \alpha_{wqa}\,\eta_{2w}\dot{\eta}_{2w} \tag{15}$$

The control law here presented has been implemented in the experimental set-up to obtain a multimodal active control of the transverse cable oscillation. However, in a first step of the analysis, only the two transversal components $\{v(\ell_m, t); w(\ell_m, t)\}$ have been measured, at the cable midspan ($x = \ell_m = \ell/2$); assuming as output the quantities,

$$\tilde{\boldsymbol{\eta}}(q_{iv}, q_{iw}) = \left\{ \begin{array}{c} \tilde{\eta}_{1v} \\ \tilde{\eta}_{1w} \end{array} \right\} = \left\{ \begin{array}{c} v(\ell_m, t) \\ w(\ell_m, t) \end{array} \right\} \simeq \left\{ \begin{array}{c} q_{1v} \\ q_{1w} \end{array} \right\} + o(q_{3v}, ...; q_{3w}, ...) \tag{16}$$

within the presented framework the EDO$_m$ control has been implemented

$$u_{EDOm}(t) = \alpha_{vl}\dot{\tilde{\eta}}_{1v}, + \alpha_{wq}\tilde{\eta}_{1w}\dot{\tilde{\eta}}_{1w} \tag{17}$$

3 Experimental model

Based on the analytical prediction, a physical model of an actively controlled cable was designed and constructed at the Dynamics and Control Lab at DISAT University of L'Aquila. A general description of the experimental setup can be found in Fig. 2. The experimental setup for active control of light cable models was built in order to furnish both the external excitation and the control force independently (see Fig. 2a). In this respect, a rigid plexiglass frame was designed and constructed to locate a control actuator able to impose a longitudinal force/displacement at one end of the suspended cable (see Fig. 2b). In order to provide smooth and continuous actions with little time delay and a high degree of dynamic efficiency in the expected frequency range of control activity, a piezoelectric actuator has been

used (Physik Instrumente, length 151 mm, open loop travel 140 μm, max voltage 1000 V, max force generation 9200 N, push/pull force capacity 4500/500 N, stiffness 66 N/m).

Moreover, the rigid frame was mounted upon an electro-dynamical shaker (Gearing & Watson V20B/PA100 (sinusoidal force peak $100N$; maximum acceleration peak 588 m/s^2; frequency range 0-14000 Hz) furnishing an imposed synchronous vertical excitation at the cable supports.

In the setup studied, the cable was built with a thin nylon wire carrying seven concentrated masses (steel balls with a diameter of 12 mm and a total added weight $w_b = 479N$). The masses were added in order to reproduce the dynamic characteristic of a selected investigated cable. The cable has a length $\ell = 500mm$ and a diameter of the cross section $\phi = 0.24$ mm; under self-weight with the steel masses it was measured to have a sag d at the midspan, with $d = 19mm$. A wire with the same characteristics was statically tested in order to measure the initial elastic extensional modulus, which has an average value of $E = 5567$ N/mm^2. The measured quantities permit, firstly, evaluation of the horizontal static component at the support, $H = 1.57$ N, and, secondly, the relevant nondimensional parameter $\mu = EA/H = 210.30$, $\nu = d/\ell = 0.038$. Consequently, the characteristic Irvine's parameter is evaluated as $\lambda^2 = 19.43$, which collocates the cable before the first crossover, classifying it as $small - sag$ (parabolic) cable.

The investigated classes of cable motion and the relative control performance primarily regard vertical symmetric forced oscillations. During the dynamic experiment the cable response has been acquired by targeting the positions of cable mid-point and lower quarter-point with an optical follower camera through analogic signal (1 Optron 5000 Hz, 2 Hamamatsu). The camera furnishes two independent signals related to vertical and horizontal components of motion that can be related either to displacements or velocities. The signals were acquired through a dSPACE 1103 PPC Controller Board. This card has 36 A/D channels usable for signal acquisition of analogic and transformation to digital data and 8 D/A channels to provide control signals to different actuators. The control loop, including I/O (ADC and DAC), can be executed with a sample rate of 300 kHz. The control loop in MATLAB/Simulink has an execution time of 1.2 μs. The dSPACE board was programmed by MATLAB and Simulink for acquisition, data visualization and control activities. In the identification and control experiments the camera signals were sampled at different time intervals ($0.001 \leq \Delta t \leq 0.005$) depending on the total acquired time interval in the experiment.

In order to identify the natural frequencies of the physical model, while avoiding misleading effects due to the non-linear system behavior, a specific test was performed exciting the model with imposed low-level vertical random motion with white Gaussian spectral properties, such that only small oscillation

amplitudes were induced.

From this data, the natural frequencies and the modal damping were clearly obtained, as reported in Table 1. The damping ratio values are in the expected range based on similar experiments [14, 15]

4 Predicted control effectiveness by analytical model

The dynamical behavior of suspended cables and the effectiveness of the proposed control strategy has been evaluated through the previosly presented analytical model. The model has been used to define the main features of the controlled cable nonlinear dynamics under in-plane harmonic force. The system response has been described through an extensive investigation conducted by means the pseudo-arclength continuation method [16, 17]. The analysis has been conducted directly on the nonlinear modal equations (9) increasing the dimension of the discretized model in order to evidence the influence of higher frequency modes in the studied dynamics due to the nonlinear modal coupling. In this respect, the higher dimensional model here considered possesses 4-*dofs* representing the first two in-plane and out-of-plane modal amplitudes, respectively. The nondimensional frequencies of the modes involved in the analysis are presented in Table 1 together with the modal damping ratios. Discrete models describing different modal interactions have been used to predict or justify the experimental observations for both uncontrolled and controlled dynamics. Those models are obtained for a selected cable for which the linear frequencies, obtained with the previously evaluated parameters μ, ν and λ^2, are close to those observed in the experimental setup (see Table 1). For this cable the response to harmonic excitation and the effectiveness of the proposed control strategies have been presented through frequency response curves of the system. The dynamic features of the cable oscillation control effectiveness, as described through the analytical model, are summarized in the folowing.

4.1 Control of in-plane motions

The presence of longitudinal control leaves the peculiarities of cable nonlinear oscillations unchanged, where an in-plane motion occurs under in-plane excitation while an out-of-plane loading produces a spatial motion. Consequently, a simple *sdof* model for the in-plane motion can be used to evaluate the control effects on planar cable motion. Frequency response curves, named in the following *frcs*, in frequency range close to the primary resonance, have been previously obtained through the multiple scale method for both highly ($\lambda^2 = 19.43$) and a moderately ($\lambda^2 = 15.36$) taut cable [9]. For the studied

moderately taut cable ($\lambda^2 = 19.43$), following the approach used in [17], a richer behavior is evidenced by performing a refined analysis using the continuation method applied directly to the modal equations of the analytical model. In particular, this approach furnishes the complete scenario at once and allows a direct comparison of the cable response at the primary and secondary (superharmonic and subharmonic) resonances.

In Fig. 3a the modification of the frequency response curve is shown for a low level of external amplitude, under different level of LC control. In this low-amplitude region the LC control effects are quite similar to those obtained adding a linear viscous damping, with negligible contribution of control quadratic terms.

Increasing the level of oscillation amplitudes, the typical distortion of the curve due to quadratic and cubic terms is observed and the emergence of counteracting nonlinear control terms [9] produces a non-proportional decrease of the oscillation amplitudes with respect to the used control gains α_{vl}, while the presence of super-harmonic resonance (3 - 3/2) in the uncontrolled case is strongly reduced by the LC control (see Fig. 3b). The typical behavior of a system possessing quadratic and cubic nonlinearities can also be evidenced showing sections at a given frequency, in the load-amplitude plane (q_{1v}, p_{1v}). The load-amplitude curve, named in the following *lac*, for a fixed frequency $\Omega = 0.8$, is shown in Fig. 3c, where the uncontrolled case clearly evidences the softening-hardening behavior increasing the load. Moreover the increase of the control gain α_{vl} modifies the curve, producing a reduction of the oscillation amplitudes in the range of a moderate level of oscillations, while for a high level of oscillations the control effectiveness is reduced up to a zero point and after that becomes undesirable. However, the curves also show the beneficial LC control effect in increasing the level of load amplitude for which the solution jumps to a high level of oscillation; indeed, the augmentation of the control gains moves the LP points (tangential bifurcations) to a high level of external amplitude. Similar behavior occurs for different frequencies (Fig. 3d).

Analysis previously conducted for in-plane symmetric quadratic control evidences certain difficulties in reducing the oscillation amplitude beyond a certain level through this control law [9]. Indeed, for a high value of the control gain, evident undesired effects appear in the low frequency range. Hence, an analysis of the feedback bilinearization has also been pursued showing that the cancelation of the elongation term increases the flexibility with consequent larger displacement, accompanied by a more regular behavior in terms of control gain effects; see [18].

Furthermore, during the experiments a bifurcation of symmetric in-plane motion into a prevailing

antisymmetric one has been observed in specific frequency ranges with a clear decrement of the effectiveness of a certain class of control laws. With the aim of reproducing such bifurcation, the response of a 2-*dofs* model including the first symmetric and anti-symmetric in-plane modes has been analyzed. The occurences of this phenomenon, deeply studied in the case of internal resonant cables [1, 20, 21], have only recently been clearly described for nonresonant cables [19]. Two regions have been defined for which the first antisymmetric mode can be involved in the dynamics through the bifurcation of the externally excited first symmetric mode with loading frequency Ω: principal unstable region ($\Omega = 2\omega_{2v}$), and second unstable region ($\Omega = \omega_{2v}$).

Here, the bifurcation of anti-symmetric motion during symmetrically-excited oscillation around the primary resonance of the first symmetric mode has been experienced in the response of both analytical and experimental models due to the closeness of the first antisymmetric mode with the second unstable region. Fig. 4a shows the *frc* obtained through the continuation method directly applied to the $2-dofs$ modal equations. Although the studied cable is not in resonance condition ($\omega_{1v} \neq \omega_{2v}$), the second unstable region, which is centered around the external frequency $\Omega = 1.25 = \omega_{2v}$, is clearly present even at a relatively low level of the external amplitude. In this narrow region the first solution branch is losing its stability through a static bifurcation in P_1 and P_2 (BP Branch Points) producing a periodic coupled motion with T-periodic modal components q_{1v} and q_{2v} with amplitudes depicted in Fig. 4a,b with respect to the forcing frequency Ω.

The description of this bifurcation is completed by increasing the load amplitude at a given frequency. The load-amplitude curves obtained at the resonant frequency $\Omega = 1.25 = \omega_{2v}$ are shown in Figs. 4 c,d. Along these curves the loss of stability of the symmetric motion is evident at the point P_5 (Fig. 4c) for a second stable branch, which admits two stable solutions for a single amplitude load value (Fig. 4d).

The analysis aims primarily to evaluate the effect of the proposed control law for cable motions in which relevant anti-symmetric components are present. The modification of the response introduced by LC control (only $\alpha_{vl} \neq 0$) shows a clear reduction of the first symmetric modal amplitude around the primary resonance. However, the frequency band of the bifurcation region involving anti-symmetric modes is unchanged, even if the anti-symmetric component appears at lower amplitude (see Figs. 4a,b). The main qualitative result obtained by the presented analysis regards the detrimental effects of the LC control for the anti-symmetric modal amplitudes (red curves in Fig. 4b). This undesired result has also been confirmed by the experimental tests when the LC control has been used. In order to avoid the amplification of the anti-symmetric component in the bifurcation region, a more complete feedback has

been considered ($\alpha_{vl} \neq 0$; $\alpha_{vq} \neq 0$). In this case the addition of a quadratic feedback depending on the anti-symmetric component permits the drastic reduction of this component with a negligible modification of the bifurcation boundaries (green curves in Figs. 4a-d).

Finally, it should be mentioned that the continuation method permits the evidencing, in the investigated region of the (p_{1v},Ω)-space, of a second bifurcation which appears for amplitudes of the first symmetric mode relatively larger than the previous one. However, the frequency range in which the bifurcation is encountered is quite large, affecting almost completely the higher part of the frc of the first symmetric mode, in the frequency range $0.8 \leq \Omega \leq 1.3$. Indeed, the first branch of solution loses stability through a period doubling (PD) bifurcation (points P_3 and P_4 on Figs. 4 a,b) due to the combination resonance $\Omega = 1/2(\omega_1 + \omega_2)$. At higher amplitude the cubic terms increase their relative importance and the $q_{2v}q_{1v}^2$-term in the anti-symmetric modal component equation produces fractional-harmonic pairs ($\frac{1}{2}\Omega, \frac{3}{2}\Omega, \frac{5}{2}\Omega$); these pairs occur in the spectrum of the anti-symmetric modal component in which the $\frac{3}{2}\Omega$ harmonic component is in resonance with the first anti-symmetric frequency (at $\Omega = 0.82$, $\frac{3}{2}\Omega \simeq \omega_{2v}$). In this case, as is evident in both the $frcs$ (Figs. 4 a,b) and the $lacs$ (Figs. 4 e,f), the LC control is effective in canceling the bifurcation mechanism, drastically reducing the first symmetric amplitude.

4.2 Control of spatial motions

The bifurcation of in-plane motion to spatial motion has also been described through the use of a 2-*dofs* discrete model, in the case of non-resonant cables. In similar cables, the effects of the dimensions of the model in the description of the cable nonlinear dynamics have been investigated through an extensive numerical campaign conducted through either path-following technique or finite element method [17]. These studies have shown that the main dynamics are well described with few modes. Here, similar analyses have been conducted for the studied case. Beside that, the effects of the proposed control strategy have been determined. Due to the nonlinear coupling between in-plane and out-of-plane modes it is known that the quadratic $q_{1w}q_{1v}$-term in the first out-of-plane modal equation can be associated to a $\frac{\Omega}{2}$ frequency content resonant with the out-of-plane natural frequency (for $\Omega \simeq 1.2$ $\frac{\Omega}{2} \simeq \omega_{1w}$). The resonant mechanism is confirmed by the results presented in Fig. 5, where the continuation procedure has been used to derive the $frcs$ to in-plane harmonic load of a 2-*dofs* model containing the first in-plane and out-of-plane modes. In Fig. 5a the response of the first in-plane mode becomes unstable through a period doubling (PD) bifurcation in the two points P_1 and P_2. Along the bifurcated branch a $2T$-periodic solution containing both the in-plane and out-of-plane components has been obtained with a

larger out-of-plane amplitude (see Fig. 5b). The section at the given fixed frequency, $\Omega = 1.2$, permits the derivation of the *lacs* reported in Fig. 5c,d where it is evident that the bifurcation load amplitude is close to zero for the given frequency. Two different controllers have been tested for reducing the spatial motion in the bifurcation region; first an LC control has been used to construct the controlled *frcs* (red line in Fig. 5). It is clear that this first control strongly reduces the in-plane component, but is ineffective in the bifurcation cancelation, leaving the out-of-plane amplitude almost unchanged. When a second out-of-plane quadratic control term is added ($\alpha_{vl} \neq 0$; $\alpha_{wq} \neq 0$), the first branch of the solution remains unchanged (the green line is superimposed to the red one), while the second bifurcated branch is strongly affected by the new control, drastically reducing the out-plane-component, and an augmentation of the in-plane component in a narrow frequency band.

The effects of the LQC control have previously been presented considering in-plane symmetric/anti-symmetric and in-plane/out-of-plane symmetric interactions; however a refined 4-*dofs* model has also been considered in the analyses. In order to demonstrate the control effectiveness in the presence of all possible interactions, a region of co-existence of symmetric and anti-symmetric modal amplitudes under in-plane loading has been selected. This co-existence region is strongly dependent on the modal damping ratio as shown in Fig. 6. For this reason an accurate numerical study has been conducted in order to select damping ratios (Model B) that are representative of the experimental cable. Fig. 6 shows the control effectiveness in the region of co-existence of in-plane symmetric and anti-symmetric modes and symmetric out-of-plane modes, considering the transition from uncontrolled to controlled motion. Figs. 6a,d,g present the time-histories obtained through direct integration of the 4-*dofs* system in a region of co-existence of three modal components (q_{1v}, q_{2v}, q_{1w}). The uncontrolled motion is characterized by a strong 2Ω component in the frequency spectra of the antisymmetric mode (q_{2v}) involved in the motion through a secondary instability ($\Omega \simeq w_{2v}$). See Figs. 6b,e,h. The introduction of an LQC control with selected positive gains ($\alpha_{vl1} = 0,3; \alpha_{vq2} = 80; \alpha_{wq1} = 80$) in equation (8), produces a sensible reduction of the forced motion with a qualitative change of the dynamics. Indeed, after the control starts, in a very short transient, the anti-symmetric components become null and the weak coupling between in-plane and out-of-plane motion behaves along a controlled U-shape trajectory with a 2T out-of-plane component (see Figs. 6c,f,i). The transition of the trajectory in the modal plane is depicted in Figs. 6l,m.

5 Control effectiveness in the experimental model

The investigated classes of cable motion and the relative control performance deal with vertical symmetric forced oscillations. The experimental set-up has been described in its entirety section 3.

After the preliminary characterization of the basic dynamic features of the physical model, several tests have been conducted to determine frequency response curves to vertical symmetric harmonic loading for an increasing level of excitation amplitude. Most of the nonlinear coupling phenomena evidenced through the analysis of the model response have also been observed in the experienced dynamics of the physical model. However, the implementation of possible control strategies has required several steps as reported in the following.

5.1 Experimental results targeting a single point

Firstly, a single-input linear control (LC) has been implemented based only on the vertical velocity of the monitored cable midspan. Varying the control gain, different levels of attenuation have been experienced in the region of the primary resonance of the first symmetric mode for a moderate level of external excitation. However, the LC control has been ineffective, or in a few situations detrimental, when the selected excitation parameters (frequency and amplitude), are such that nonlinear coupling between in-plane and out-of-plane or symmetric and anti-symmetric modes are present.

The *EDOm* control, based on two inputs, in-plane and out-of-plane midspan components, has been successively implemented. This direct control feedback behaves similarly to the nonlinear polynomial control (LQC_{out}, see equation (10)) and it is implemented assuming that the measured transversal components are substantially contributed only by the first in-plane and out-of-plane modes, respectively. The control strategy shows a great ability to reduce prevailing symmetric cable spatial motion. The obtained response reduction depends quantitavely on the control gains; here, for sake of brevity, a single measured dynamics is presented as shown in Fig. 7. The recorded time histories of the two midspan displacement components evidences the immediate effect obtainable upon starting the control (Figs. 7a,d). A spectral analysis conducted on the uncontrolled interval confirms that the bifurcation in spatial motion of the in-plane excited dynamics is occuring through a period doubling for the physical model also. Indeed, the Fourier spectra in Figs. 7b,e of the in-plane components possess mainly the forcing frequency (f=5.97 Hz), while the out-of-plane displacement spectrum possesses a lower harmonic component at half of the external frequency (f=2.99 Hz). After the encouraging presented preliminary results, a larger experi-

mental campaign has been conducted varying both the frequency and the amplitude of the symmetric forcing load in order to classify the region of coupled symmetric in-plane/out-of-plane motion. In the uncontrolled case the experienced region of coupling is summarized through Fig. 8a, in which the stability margins between single mode in-plane motion (cross) and coupled symmetric in-plane/out-plane motion (dots) are depicted in the frequency-amplitude plane of the external excitation. Fig. 8b show the new stability margins evaluated when the EDO_m control was activated. A direct comparison of the two presented results evidences the reduction of the unstable region where spatial motion occurs. Representing the uncontrolled *vs* controlled response for a given external load permits the evaluation of the experimental *frcs* to in-plane excitation as is given in Figs. 8c. Here, following the black line, a prevailing in-plane motion is evident, coupled in a relatively narrow frequency range $(5,8 < f[Hz] < 6,3)$ with a smaller out-of-plane component. In the presence of the EDO_m control (equation (17)), the *frc* of the measured midspan in-plane component is strongly reduced up to the external frequency of 6 Hz, increasing its amplitude for larger frequencies. The augmentation of motion amplitude is accompanied by a strong anti-symmetric component which was immediately visible in the experiment. The experienced large region of control inefficiency has suggested the introduction of a multimodal control based on a direct measuring of two points as further presented.

5.2 Experimental results targeting two points

Notwithstanding the promising obtained EDO_m control performance, the experimental tests have clearly evidenced the inability of this control to reduce the amplitude of motions with prevailing anti-symmetric components. Consequently, the full (EDO) control (see equation (15)) has been introduced and successively implemented in the experimental prototype. The performance obtained by this control is here briefly summarized, presenting the control effects on the *frcs* to in-plane excitation of transversal displacement of the cable quarter. The *frcs* of the tested physical model are obtained by moving the frequency, back and forward, from low to high frequency values and measuring the response of the system. Figs. 9 show the experimental *frcs* for a relatively low value of the excitation amplitude. In the uncontrolled case, the response shows two regions of resonance, the primary resonance of the first symmetric mode with external frequency close to its frequency ($f \simeq f_{1v} = 5.92Hz$), and the second resonance of the anti-symmetric mode with external frequency close to this last one ($f \simeq f_{2v} = 7.2Hz$). For a given selection of the EDO control gains, a considerable reduction of the dynamic response has been obtained in the whole experienced frequency range around the primary resonance, with a single exception in the

point P_1 (see Fig. 9a). This singular point is characterized by a superharmonic resonance with the third mode ($f \simeq f_{3v}/2$). In this case the uncontrolled peak (point P_1) is amplified by the control (point P_2). At the primary resonance, the *EDO* control permits a strong regularization of the periodic motion as is visible in comparing the uncontrolled *vs* controlled (black *vs* red) motion, and comparing the orbits in the (v,w)-plane. It is clear that in the uncontrolled case a small coupling between symmetric in-plane and out-of-plane motion is present in the global dynamics. This coupling is completely suppressed by the *EDO* control at the primary resonance.

The results of the experienced transition from uncontrolled to controlled motion in the region of the primary in-plane resonance are summarized in Figs. 10 in which the strongly-coupled spatial motion is reduced to a small in-plane motion when the *EDO* control is activated. Indeed, the time-histories in Figs. 10a,d show the strong reduction of the out-of-plane component confirmed by the cancelation of the frequency component $f/2$ (Figs. 10c,f) present in the spectrum of the uncontrolled motion (Figs. 10b,e).

In the region of the anti-symmetric modes ($f \geq 7.0\ Hz$) a series of experiments have been conducted in order to evaluate the sensitivity of the response to the variation of the control gains. A sensible reduction of the anti-symmetric in-plane and out-of-plane amplitudes has been obtained as depicted in Figs. 11, where the control effects on the response at the cable quarter are presented. In the uncontrolled response two branches of solution have been classified; at lower frequency a spectral analysis of the response has shown a quasi-periodic behavior which becomes periodic in the second higher branch of solution. The control leaves these motion characteristics unchanged; however, lower amplitudes are recorded associated with smaller orbits in the (v,w)-plane.

Also, in the region of prevailing anti-symmetric modal dynamics, the transition from uncontrolled to controlled motion has been investigated and the results for a selected case are reported in Figs. 12. The time-histories show in this case a complicated transient in which in some instances the out-of-plane component exceeds the uncontrolled one (see Figs.12a,d). However, looking at either the frequency component evaluated in the intervals before (Figs.12b,e) and after (Figs.12c,f) the control start or the orbit in the (v,w)-plane, the *EDO* control effectiveness can be easily appreciated. In particular, considering the symmetric and anti-symmetric components of the motion as it is shown in Figs.12h,i the efficiency of the experimental apparatus for a multimodal control is confirmed.

Conclusions

Multimodal active control of cable oscillations through a longitudinal action has been fully exploited both through analytical-numerical models and experimental prototypes. On the basis of a classical analytical model for nonlinear cable oscillations, different methodologies in the design of suitable control feedbacks have been presented. Full state-feedbacks have been proposed with the aim of producing an asymptotically-stable system in the case of bilinearization, or a dissipative system controlled by an opportune polynomial nonlinear feedback.

Furthermore, the main research findings here presented deal with the validation through a physical model, of the ability of longitudinal active control in stabilizing nonlinear cable oscillations. In this respect, an implementable noncollocated control law based on direct-output feedback has presented showing that this approach preserves all the features of the previously-developed control methodologies. Notwithstanding the motion coupling, a noncollocated control law based on the independent measures of both in-plane and out-of-plane response shows good ability to reduce in-plane and out-of-plane oscillations simultaneously.

Different refined reduced discrete models, with an increasing number of modes, have been used to demonstrate the performance of the selected control laws numerically. These analyses have been driven by the dynamics experienced in the laboratory tests. Indeed, despite the nominal absence of internal resonances for the selected cable, a small-sag parabolic cable, the experienced dynamics under in-plane harmonically-forced oscillations has shown a rich and evident modal coupling between the first two in-plane and two out-of-plane modes. The main modal interaction phenomena have been described constructing the frequency response curves *frcs* to the in-plane symmetric load for models containing an increasing number of modes. The *frcs* have been determined by the pseudo-arclength continuation method, in order to describe the bifurcation points and the post-critical branches of solutions.

Further, the effects of the proposed control law are also presented examining the modification added by the control to the *frcs*. The numerical findings have been confirmed by experimental results showing that in a wide experienced frequency range of the external force, around the primary resonance of the first symmetric mode, a rich modal interaction can be found even in absence of internal resonance conditions. Thus, a motion mainly described by a symmetric in-plane mode can easily be coupled with the symmetric out-of-plane mode and, in the proximity of the explored frequency region, also with the first anti-symmetric in-plane and out-of-plane modes. These modal components are opportunely desumed by the experimental measures, obtained at two points, $\ell/4$ and $3/4\ell$, with two biaxial follower cameras. The

control strategy based on a single longitudinal action driven by the direct-output nonlinear feedback, on the basis of the four measured transverse components, has shown control capability in the entire experienced frequency range overcoming all the encountered motions from the classical symmetric in-plane type to more complicated spatial motion with the presence of both symmetric and anti-symmetric components.

Acknowledgments

The research has been supported through Italian national project COFIN 03-04 titled *Dynamics of Flexible Structures* and Italian national project COFIN 04-05 titled *Vinces - Vibrations IN Civil Engineering Structures*.

References

[1] G. Rega, Nonlinear vibrations of suspended cables - Part I: Modeling and analysis - Part II: Deterministic phenomena , Appl. Mech. Rev. 57 (2004) 443, 479.

[2] R.E. Christenson, B.F. Spencer, E.A. Johnson, Experimental verification of smart cable damping. ASCE J. Engrg. Mech., 132 (2006) 268.

[3] B.M. Pacheco, Y. Fujino, A. Sulekh, Estimation curve for modal damping in stay cables with viscous damper. ASCE J. Struct. Eng., 119 (1993) 1961.

[4] C.F. Baicu, C.D. Rahn, B.D. Nibali. Active boundary control of elastic cables: theory and experiments. J. Sound and Vibr. 198 (1996) 17.

[5] H. Canbolat, D. Dawson, C.D. Rahn, S. Nagarkatti, Adaptive boundary control of out-of-plane cable vibration. J. Appl. Mech. 65 (1998) 963.

[6] Y. Fujino, P. Warnitchai, B. M.Pacheco, Active stiffness control of cable vibration. ASME J. of Appl. Mech., 60 (1993) 984.

[7] T. Susumpow and Y. Fujino, Active control of multimodal cable vibrations by axial support motion. ASCE J. of Eng. Mech., (1995) 121, 964.

[8] Y. Achkire and A. Premount, Active tendon control of cable-stayed bridges. Earth. Eng. and Str. Dyn., 25 (1996) 585.

[9] V. Gattulli, M. Pasca and F. Vestroni, Nonlinear oscillations of a nonresonant cable under in-plane excitation with a longitudinal control. Nonl. Dyn., 14 (1997), 139.

[10] R. W. Gehle, S. F. Masri. Active control of shallow, slack cable using the parametric control of end tension. Nonl. Dyn., 17 (1997) 77.

[11] V. Gattulli, F. Vestroni, Nonlinear strategies for longitudinal control in the stabilization of an oscillating suspended cable. Dyn. & Contr., 10 (2000) 359.

[12] A. Luongo, G. Rega, F. Vestroni, Planar nonlinear free vibrations of elastic cable. Int. J. of Non-linear Mech. 19 (1984), 39.

[13] A. Benallou, D. A.Mellichamp and D. E.Seborg. Optimal stabilizing controllers for bilinear systems. *Int. J. of Control,* vol. 48, pp. 1487–1501, 1988.

[14] G. Rega, R. Alaggio, Spatio-temporal dimensionality in the overall complex dynamics of an experimental cable/mass system, Solid and Structures, 38 (2001) 2049.

[15] V. Gattulli, M. Lepidi, J. Macdonald, C. Taylor, One-to-two global-local interaction in a cable-stayed beam observed through analytical, finite element and experimental models, Int. Journal of Non-Linear Mechanics, 40(5) (2005) 571.

[16] E. Doedel and J. P.Kernevez AUTO: Software for continuation and bifurcations problem in ordinary differential equations. *Applied Math. Report, California Institute of Technology, 1986*

[17] V. Gattulli, L. Martinelli, F. Perotti, F. Vestroni, Nonlinear oscillations of cables under harmonic loading using analytical and finite element models, Computer Methods Applied Mechanics & Engineering 193 (2004) 69.

[18] V. Gattulli, F. Vestroni, Nonlinear feedback control strategies for an oscillating suspended cable, International Conference on Control of Oscillations and Chaos (COC97), August 27-29, S.Petersburg, Russia, 1997.

[19] K. Takahashi, Q. Wu, S. Nakamura, In-plane antisymmetric response of cables through bifurcation under symmetric sinusoidally time-varying load, J. Sound Vib. 268 (2003) 1.

[20] G. Rega, W. Lacarbonara, A.H. Nayfeh, C.M. Chin, Multiple resonances in suspended cables: direct versus reduced-order models, Internat. J. Non-Linear Mech. 34 (1999) 901.

[21] G. Rega, W. Lacarbonara, Resonant non-linear normal modes. Part II: activation/orthogonality conditions for shallow structural systems, Internat. J. Non-Linear Mech. 38 (2003) 873.

[22] F. Benedettini, G. Rega, R. Alaggio, Nonlinear oscillations of a four-degree-of freedom model of a suspended cable under multiple internal resonance conditions. J Sound Vib. 182 (1995) 775.

[23] H. M. Irvine, Cable Structures, The MIT Press, Cambridge, (1981).

Appendix

A non-dimensional form of eqs. (5) can be obtained introducing the following quantities:

$$\begin{aligned} &\tilde{x} = \frac{x}{l}, \quad \tilde{y} = \frac{y}{d}, \quad \tilde{v} = \frac{v}{\ell}, \quad \tilde{w} = \frac{w}{\ell}, \quad \tilde{\omega}_{iv} = \frac{\omega_{iv}}{\omega_{1v}}, \quad \tilde{\omega}_{iw} = \frac{\omega_{iw}}{\omega_{1v}}, \\ &\tau = \omega_{1v} t, \quad \mu = \frac{EA}{H}, \quad \nu = \frac{d}{\ell}, \end{aligned} \tag{18}$$

The modal shapes of a suspended cable are given by the following expressions:

$$\begin{aligned} \varphi_i(x) &= \left(1 - \tan\frac{\beta_i}{2}\sin\beta_i x - \cos\beta_i x\right) b_i, \ i = 1, 3, \ldots (symmetric) \\ \varphi_i(x) &= \sin i\pi x, \ i = 2, 4, \ldots \quad (asym) \\ \psi_k(x) &= \sin k\pi x, \ k = 1, 2, 3, \ldots \end{aligned} \tag{19}$$

where $b_i = \cos\frac{\beta_i}{2}\frac{1}{\cos\beta_i + (-1)^h}$ is a normalization constant ($h = i$ for $i = 1, 5, \ldots$ and $h = 2i$ for $i = 3, 7, \ldots$) and the spatial frequencies β_i are given by the roots of the characteristic equation

$$\tan\frac{\beta_i}{2} - \left[\frac{\beta_i}{2} - \frac{4}{\lambda^2}\left(\frac{\beta_i}{2}\right)^3\right] = 0 \tag{20}$$

which depend on Irvine parameter $\lambda^2 = 64\mu\nu^2$, with μ and ν given by equations (18), [23] while the related dimensional natural frequencies can be obtained as:

$$\begin{aligned} \omega_{iv} &= \frac{\beta_i}{\pi}\omega_s, \ i = 1, 3, \ldots \ (sym) \qquad \omega_{iv} = i\omega_s, \ i = 2, 4, \ldots \ (asym) \\ \omega_{iw} &= i\omega_s, \ i = 1, 2, 3, \ldots, \qquad \text{where } \omega_s = \frac{\pi}{\ell}\sqrt{\frac{H}{m}} \end{aligned} \tag{21}$$

In order to define the coefficients of eqs. (8)(13), let us introduce the following integrals:

$$
\begin{aligned}
I_i^m &= \int_0^1 f_i^2(x)\,dx, \quad I_{ij}^e = \int_0^1 f_i'(x) f_j'(x)\,dx, \quad I_{ij}^a = \int_0^1 f_i(x) f_j(x)\,dx, \\
I_i^y &= \int_0^1 y'(x)\, f_i'(x) dx, \quad I_i^p = \int_0^1 f_i(x) dx
\end{aligned} \tag{22}
$$

where f_i and f_i' are the placeholders of $\varphi_i(x)$, or $\psi_i(x)$ and their derivatives where appropriate, and $y(x)$ is the parabolic function lying in the vertical plane. Consequently, the coefficients a_{ij} and b_{ij}, the damping coefficients $\zeta_{ij} = \zeta_{ij}^m$ of the damping matrix, in eqs. (8)(13) are defined as follows :

In-plane equations

$$
\begin{aligned}
&\zeta_{ijv} = \frac{\mu_v}{m\omega_{1v}}\delta_{ij}, \qquad p_i = \frac{I_i^p}{I_i^{mv}} \\
&a_{0ij} = \frac{I_{ij}^{ev}}{I_i^{mv}}\frac{1}{\beta_1^2}\,, \qquad a_{1i} = \mu\nu\frac{I_i^{yv}}{I_i^{mv}}\frac{1}{\beta_1^2}\,, \qquad a_{2ij} = \mu\frac{I_{ij}^{ev}}{I_i^{mv}}\frac{1}{\beta_1^2}\,, \\
&b_{1j} = \nu I_j^{yv}\,, \qquad b_{2ij} = \frac{1}{2}I_{ij}^{ev}\,, \qquad b_{3i} = \frac{1}{2}I_{ii}^{ew}\,,
\end{aligned} \tag{23}
$$

Out-of-plane equations

$$
\begin{aligned}
&\zeta_{ijw} = \frac{\mu_w}{m\omega_{1v}}\delta_{ij}, \\
&\omega_{iw}^2 = \frac{I_{ii}^{ew}}{I_{ii}^{mw}}\frac{1}{\beta_1^2}\,, \qquad a_{3i} = \mu\frac{I_{ii}^{ew}}{I_{ii}^{mw}}\frac{1}{\beta_1^2}\,, \\
&b_{1i} = \nu I_j^{yv}\,, \qquad b_{2ij} = \frac{1}{2}I_{ij}^{ev}\,, \qquad b_{3i} = \frac{1}{2}I_{ii}^{ew}\,,
\end{aligned} \tag{24}
$$

where δ_{ij} is the Kronecher operator and the apexes of the integrals I define completely the type of functions integrated, according to eqs. (22), together with the use of symbols v and w as indicators of the used eigenfunctions $\varphi_i(x)$ or/and $\psi_i(x)$, respectively.

Table 1: In-plane and out-of-plane frequencies and damping ratios of the cable models

Frequency f	In	$1v_s$	$2v_a$	Out	$1w_s$	$2w_a$
$ModelA$		1.000	1.253		0.627	1.253
$ModelB$		1.000	1.253		0.627	1.253
$ModelC$		1.000	1.229		0.627	1.238
Damping ξ	In	$1v_s$	$2v_a$	Out	$1w_s$	$2w_a$
$ModelA$		0.025	0.009		0.020	0.010
$ModelB$		0.027	0.0003		0.00215	0.0008
$ModelC$		0.025	0.001		0.002	0.001

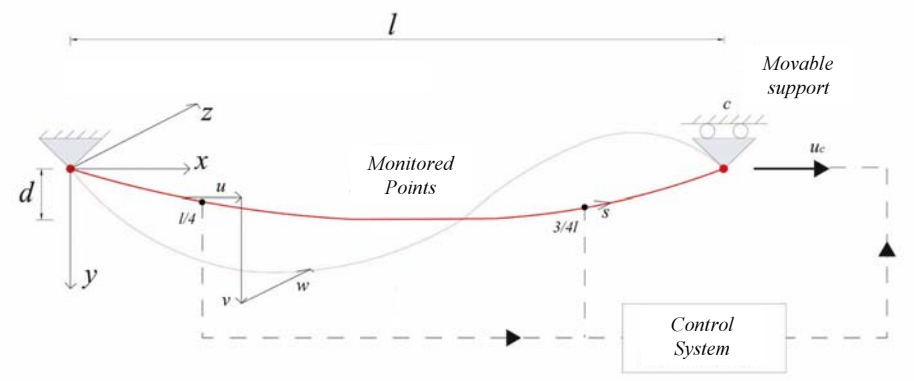

Figure 1: Cable configuration and control feedback.

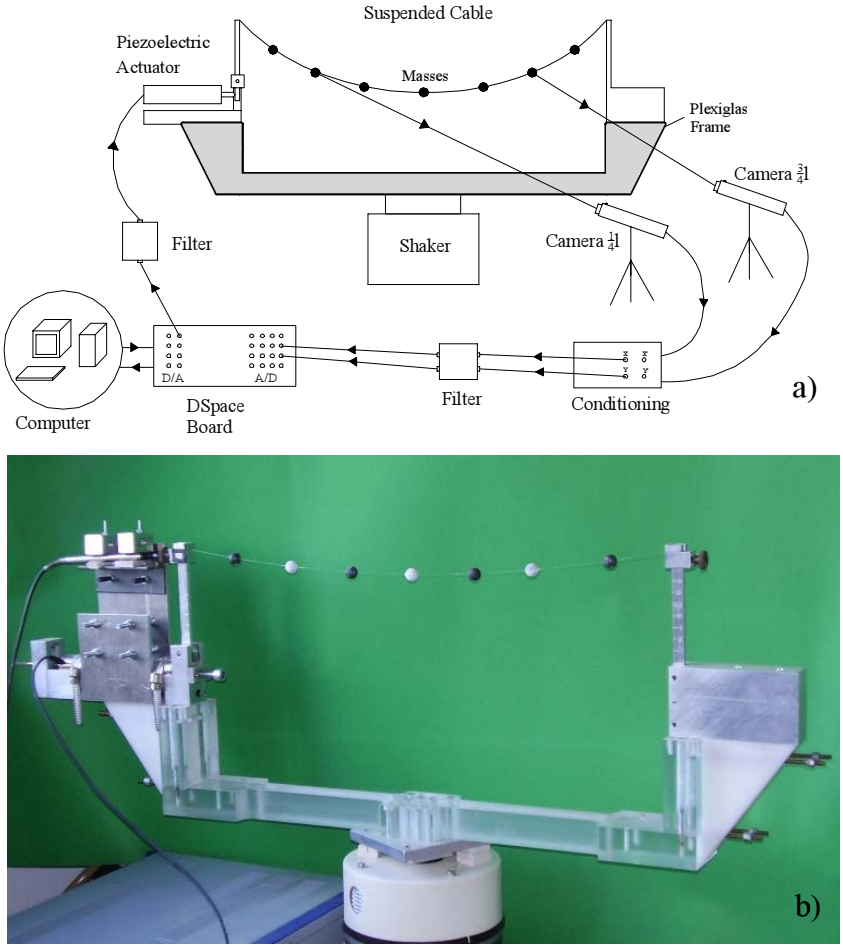

Figure 2: Experimental setup: (a) sketch, (b) lateral view

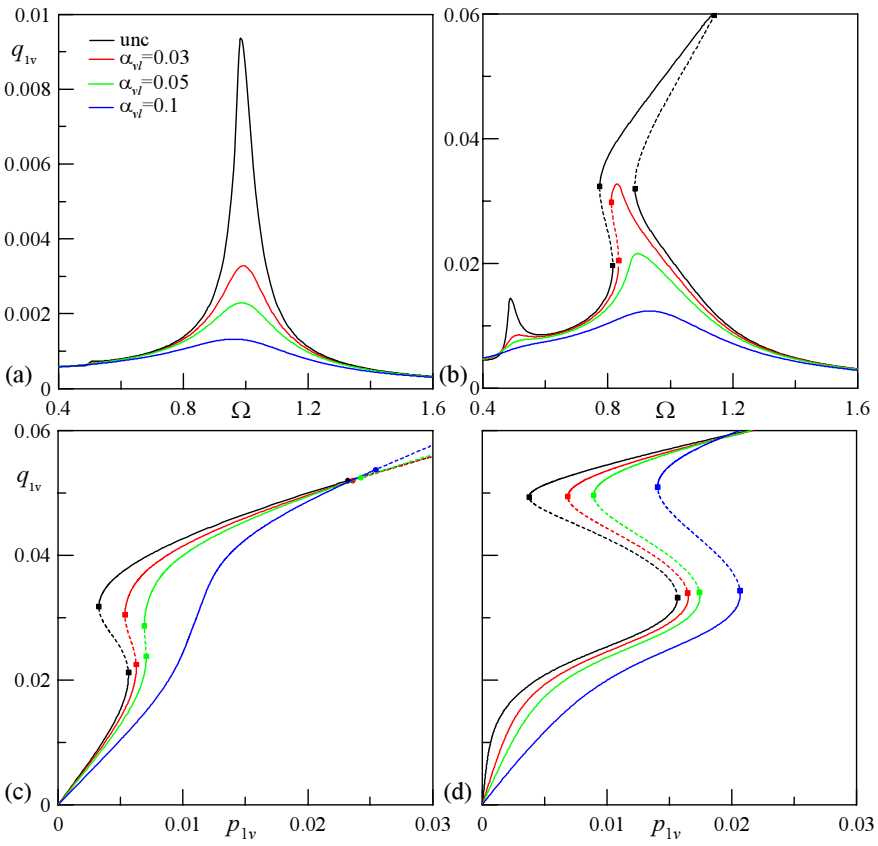

Figure 3: Cable response and control effectiveness evaluated through a *sdof* model: *frcs* to in-plane symmetric harmonic load (a) $p_{1v} = 0.0005$, (b) $p_{1v} = 0.005$; *lacs* at given loading frequency (c) $\Omega = 0.8$,(d) $\Omega = 1.0$

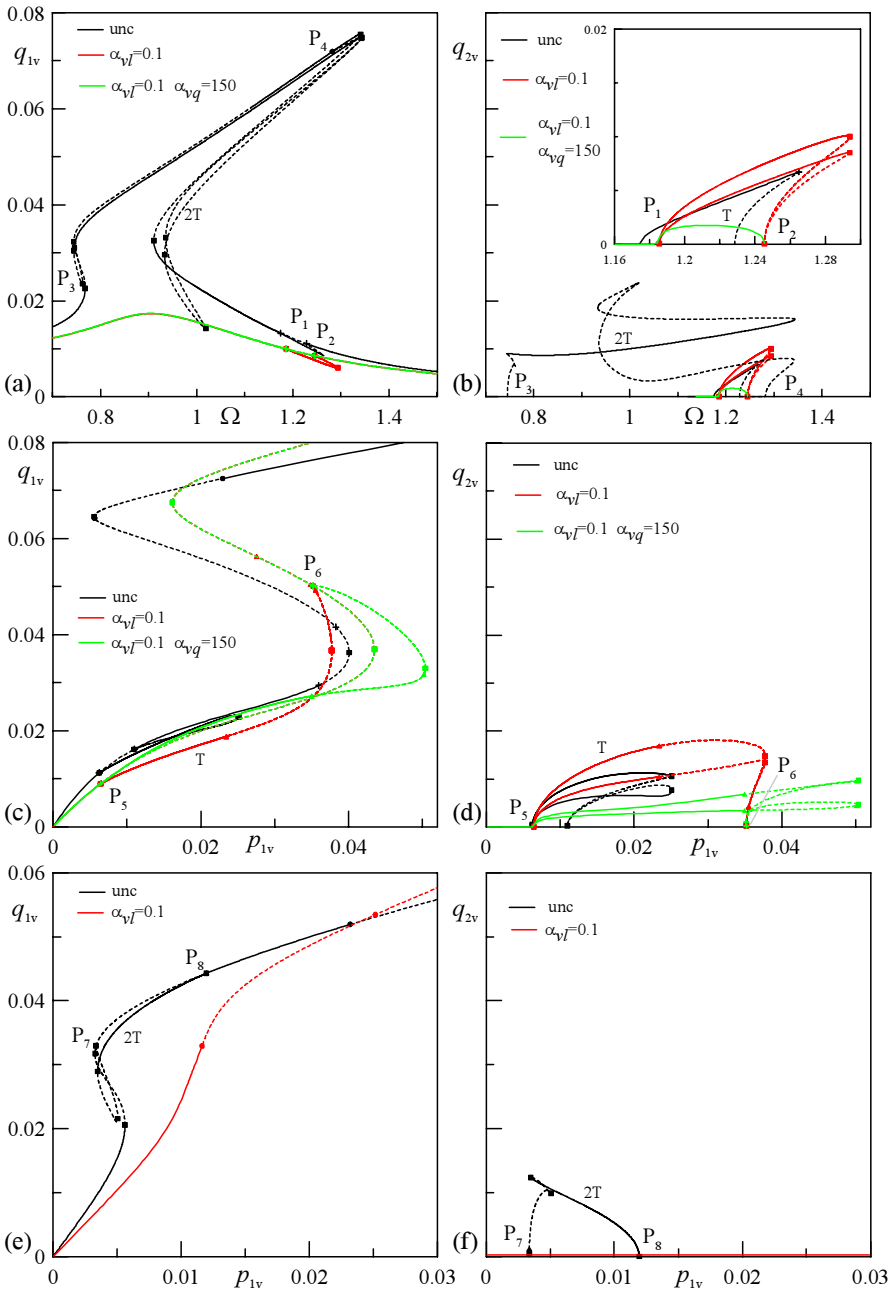

Figure 4: Planar cable response and effectiveness of linear symmetric (LC red line) and linear symmetric and quadratic antisymmetric (LQC_{in} green line) control feedbacks evaluated through a $2dof$ model: $frcs$ to in-plane symmetric harmonic load for $p_{1v} = 0.007$; (a) 1^{st} and 2^{nd} branches of q_{1v}-amplitude; (b) 2^{nd} branch of q_{2v}-amplitude; $lacs$ at given loading frequency; 1^{st} and 2^{nd} branches of the q_{1v}-amplitude , (c) $\Omega = 1.0$, (e) $\Omega = 1.25$; 2^{nd} branches of the q_{2v}-amplitude, (d) $\Omega = 1.0$, (f) $\Omega = 1.25$

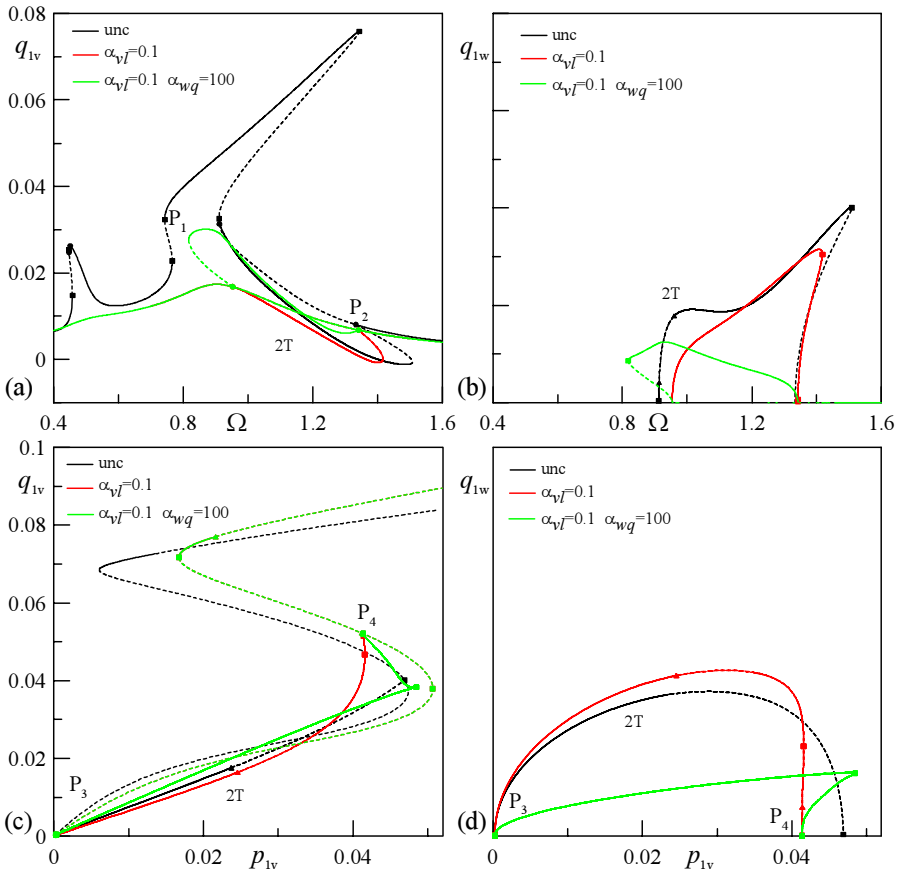

Figure 5: Spatial cable response and effectiveness of linear symmetric in-plane (LC red line) and linear symmetric in-plane and quadratic symmetric out-of-plane (LQC_{out} green line) control feedbacks evaluated through a $2dof$ model: $frcs$ to in-plane symmetric harmonic load for $p_{1v} = 0.007$; (a) 1^{st} and 2^{nd} branches of q_{1v}-amplitude ; (b) 2^{nd} branch of q_{1w}-amplitude; $lacs$ at given loading frequency $\Omega = 1.2$; (c) 1^{st} and 2^{nd} branches of the q_{1v}-amplitude , (d) 2^{nd} branches of the q_{1w}-amplitude.

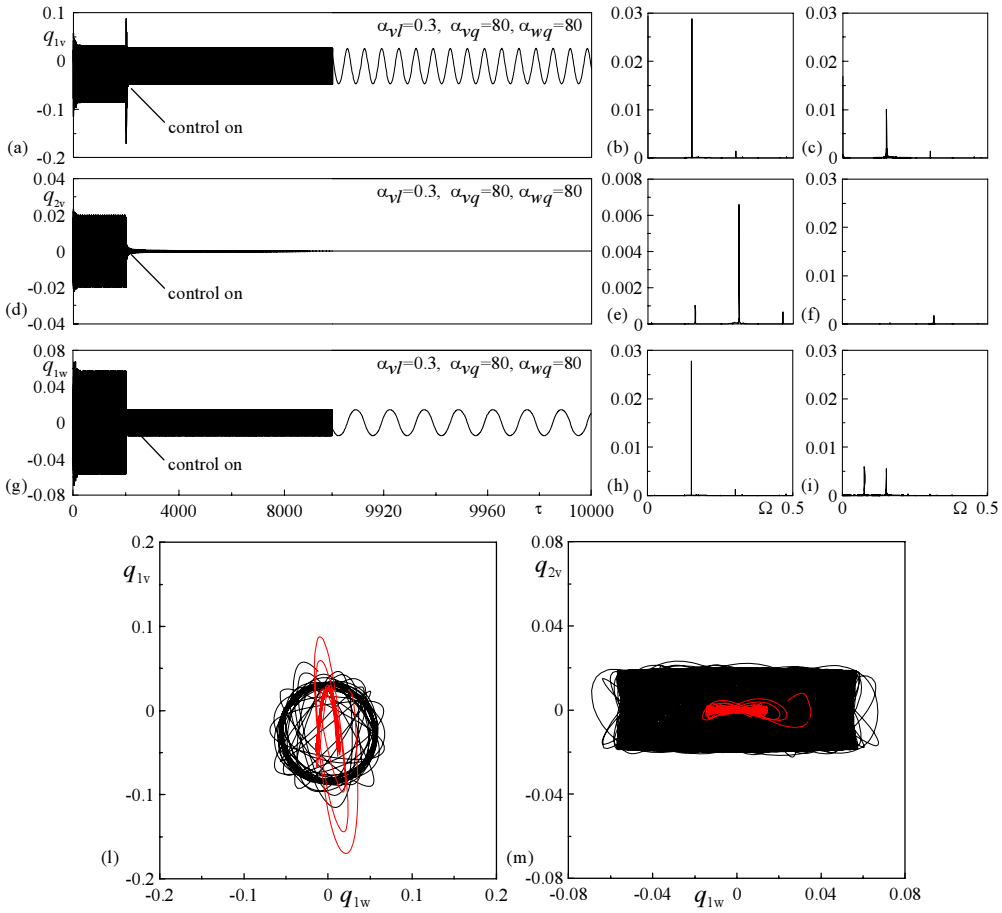

Figure 6: Numerical time histories of forced oscillations ($\Omega = 0.95$; $f_{1v} = 5.92Hz$) during the transition to controlled motion evaluated through a $4 - dofs$ model: (b) (e) (h) FFT of the uncontrolled interval; (c) (f) (i) FFT of the controlled interval.

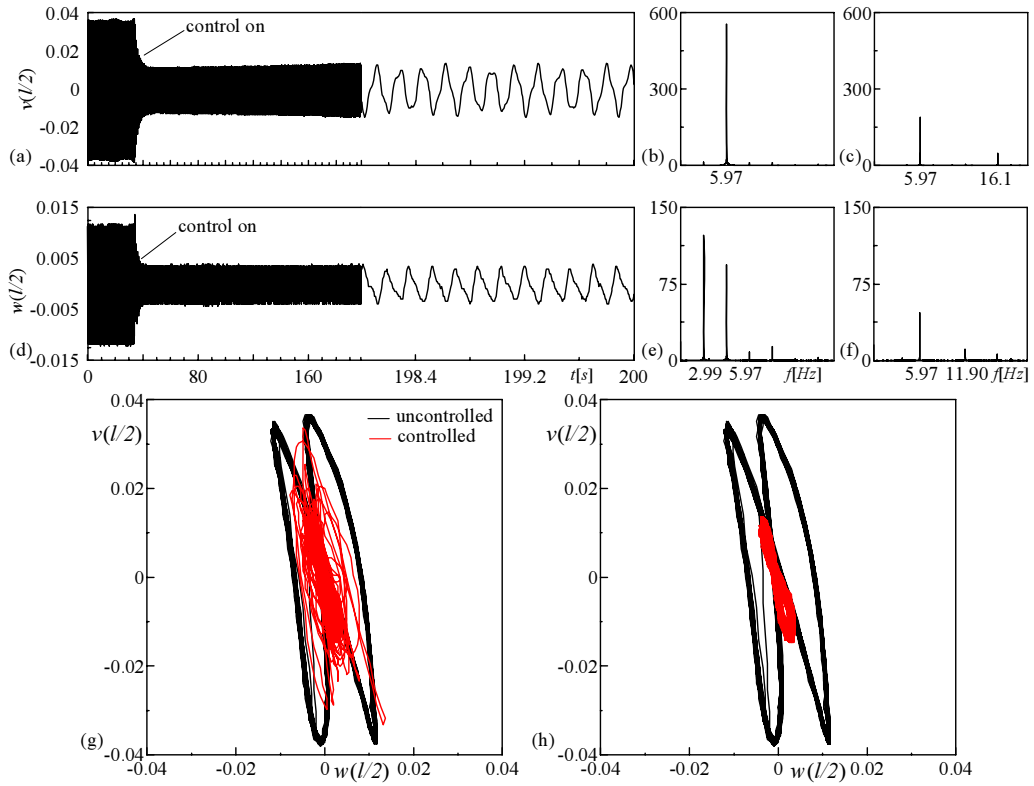

Figure 7: Experimental time histories of forced oscillations ($\Omega = 1.008$; $f_{1v} = 5.92Hz$) during the transition to LQC_{out} controlled motion: (a) (d) midspan transversal displacements; (b) (e) FFT of the uncontrolled interval; (c) (f) FFT of the controlled interval; (g) (h)

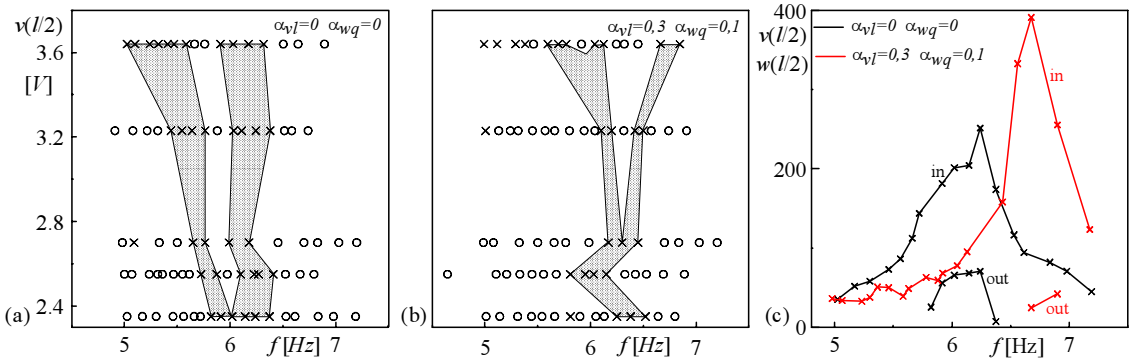

Figure 8: Effects of EDO$_m$ control based on a single measured point in the response of an experimental cable (Model C): forcing amplitude-frequency map for uncontrolled (a) and controlled (b) case; (c) experimental $frcs$ for uncontrolled and controlled case.

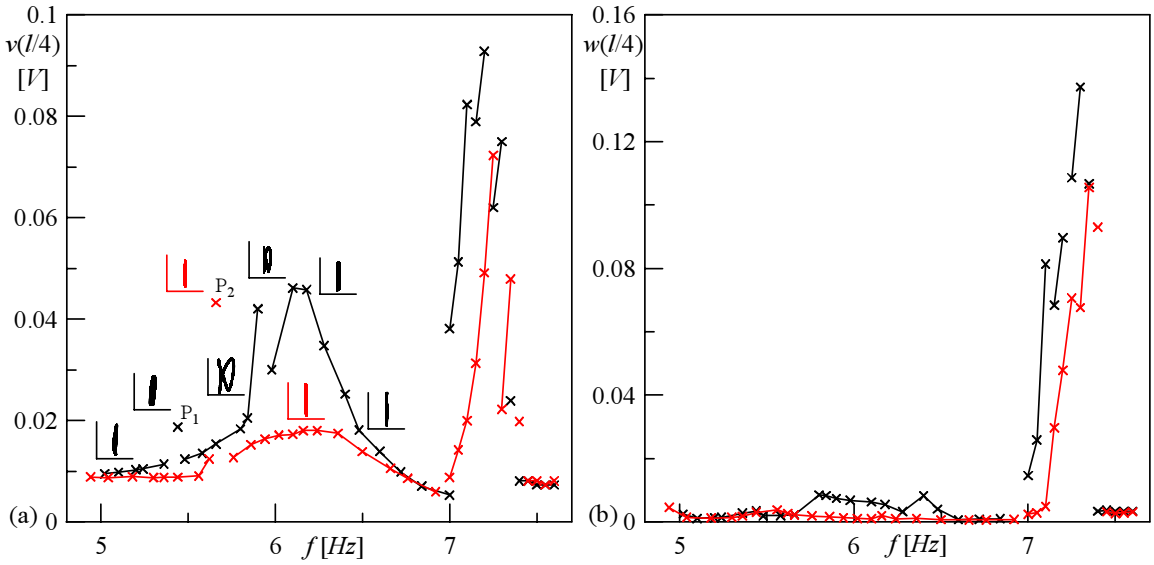

Figure 9: Effects of EDO control on experimental $frcs$ of in-plane (a) and out-of-plane (b) transversal displacement at a quarter-point to in-plane harmonic loading of an experimental cable (Model C) in the region around the primary resonance ($\Omega \simeq w_{1v}$) and the secondary resonance ($\Omega \simeq w_{2v}$).

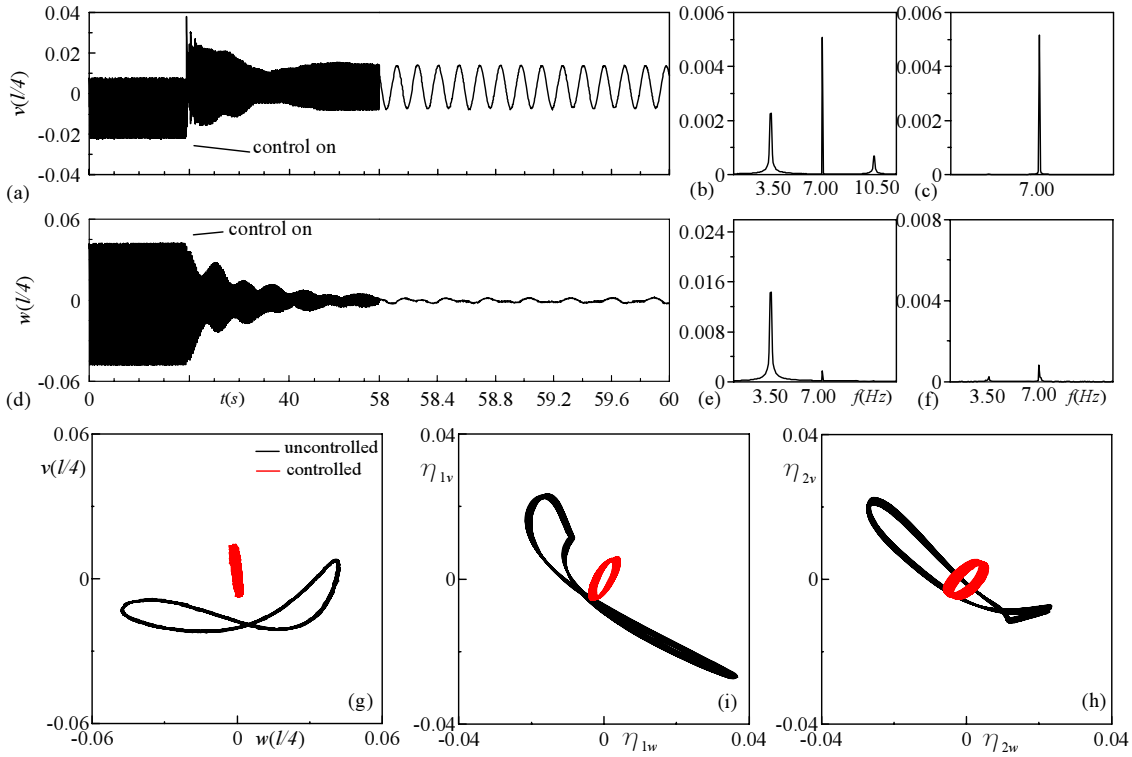

Figure 10: Experimental time histories of forced oscillations ($\Omega = 1.18$; $f_{1v} = 5.92Hz$) for an experimental cable (Model C) to MLQC controlled motion: (a) (d) transversal displacement of a quarter-point; (b) (e) FFT of the uncontrolled interval; (c) (f) FFT of the controlled interval; (g) orbits; (h) anti-symmetric components; (i) symmetric components.

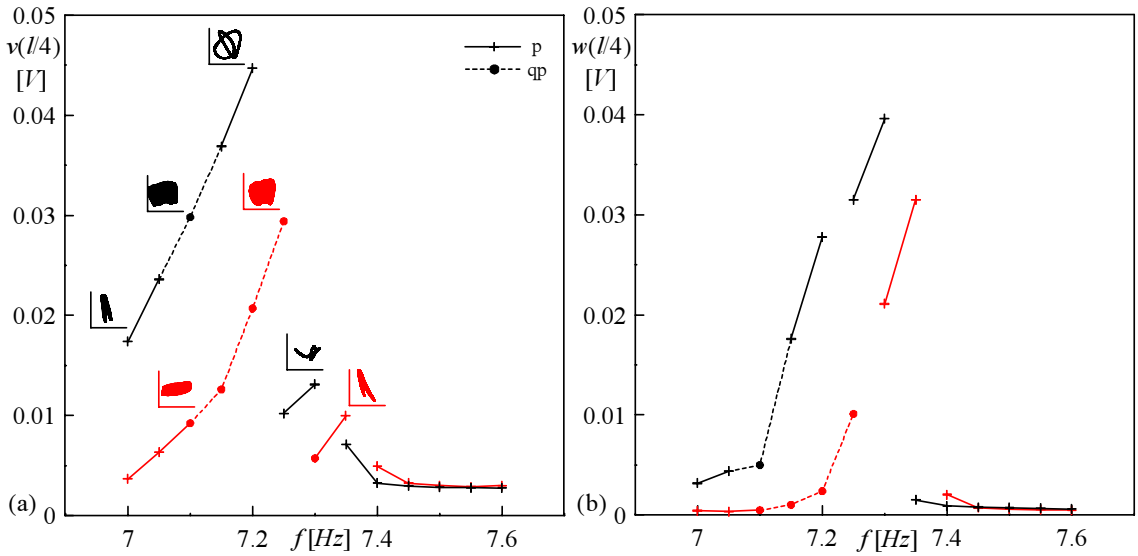

Figure 11: Effects of EDO control on experimental $frcs$ of in-plane (a) and out-of-plane (b) transversal displacement at a quarter-point to in-plane harmonic loading of an experimental cable (Model C) at the secondary resonance of the first anti-symmetric in-plane frequency ($\Omega \simeq w_{2v}$).

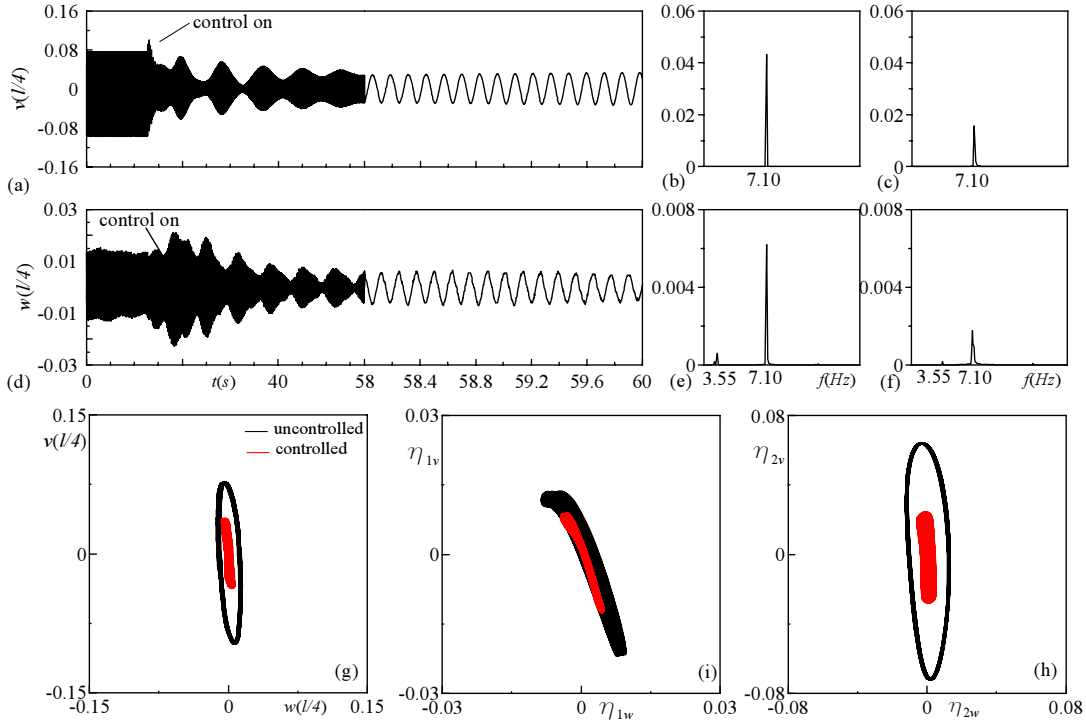

Figure 12: Experimental time histories of forced oscillations ($\Omega = 1.32$; $f_{1v} = 5.92Hz$) for an experimental cable (Model C) to EDO controlled motion: (a) (d) transversal displacement of a quarter-point; (b) (e) FFT of the uncontrolled interval; (c) (f) FFT of the controlled interval; (g) orbits; (h) anti-symmetric components; (i) symmetric components.